ACS NANO

www.acsnano.org

ARTICLE

Control of Monodomain Polymer-Stabilized Cuboidal Nanocrystals of Chiral Nematics by Confinement

Monirosadat Sadati,[#] Jose A. Martinez-Gonzalez,[#] Alexander Cohen, Sepideh Norouzi, Orlando Guzmán, and Juan J. de Pablo*

Cite This: *ACS Nano* 2021, 15, 15972−15981

Read Online

ACCESS | Metrics & More | Article Recommendations | Supporting Information

ABSTRACT: Liquid crystals are important components of optical technologies. Cuboidal crystals consisting of chiral liquid crystals—the so-called blue phases (BPs), are of particular interest due to their crystalline structures and fast response times, but it is critical that control be gained over their phase behavior as well as the underlying dislocations and grain boundaries that arise in such systems. Blue phases exhibit cubic crystalline symmetries with lattice parameters in the 100 nm range and a network of disclination lines that can be polymerized to widen the range of temperatures over which they occur. Here, we introduce the concept of strain-controlled polymerization of BPs under confinement, which enables formation of strain-correlated stabilized morphologies that, under some circumstances, can adopt perfect single-crystal monodomain structures and undergo reversible crystal-to-crystal transformations, even if their disclination lines are polymerized. We have used super-resolution laser confocal microscopy to reveal the periodic structure and the lattice planes of the strain and polymerization stabilized BPs in 3D real space. Our experimental observations are supported and interpreted by relying on theory and computational simulations in terms of a free energy functional for a tensorial order parameter. Simulations are used to determine the orientation of the lattice planes unambiguously. The findings presented here offer opportunities for engineering optical devices based on single-crystal, polymer-stabilized BPs whose inherent liquid nature, fast dynamics, and long-range crystalline order can be fully exploited.

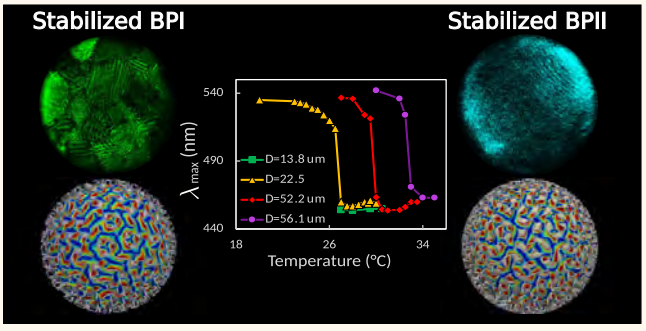

KEYWORDS: *liquid crystals, photonic soft crystals, stabilized blue-phases, confinement, confocal microscopy*

INTRODUCTION

Precise control of crystal growth and crystal transformations is central to science and engineering.[1−3] Here, we present a strategy to produce stabilized soft, macroscopic single crystals consisting of polymerized versions of the so-called blue phase (BP) liquid crystals.[4] We polymer stabilize BPs within spherical confinement. The resulting stabilized BP crystals exhibit distinct droplet-size correlated behavior and undergo reversible transformations between different structures, which can be triggered by either physical or chemical means. Confinement is shown to have a marked effect on the transition temperatures of the polymer-stabilized material, where micron-scale variations of the radius lead to temperature changes of several degrees. This high sensitivity offers opportunities for the design of stimuli responsive soft photonic crystals.

BPs are high chirality liquid crystals that exhibit cubic-crystalline symmetries, with submicron lattice parameters and Bragg refraction of visible light. The hybrid liquid-order properties of BP soft crystals make them ideal candidates for photonics and biosensing applications under conditions where traditional atomic solid crystals cannot be employed.[4−13] BPs share many similarities with atomic crystals, including long-range molecular order and the ability to undergo crystal−crystal transformations.[4−6] BP molecules are locally organized into double-twisted cylinders (DTCs), wherein the local

Received: May 18, 2021
Accepted: September 22, 2021
Published: October 1, 2021

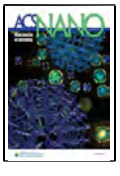

https://doi.org/10.1021/acsnano.1c04231
ACS Nano 2021, 15, 15972−15981

molecular alignment, which is represented by a vector commonly referred as the local nematic director (n), radially rotates with respect to the cylindrical axis. DTCs may assemble into a body-centered cubic (bcc) symmetry to produce the BPI or a simple-cubic (sc) symmetry to form the BPII. The crystalline assembly of DTCs is interspersed by distinct disclination (defects) lines. It is generally more convenient to visualize BPs by showing the characteristic array of topological line defects (Figure 1a) that percolates their structure.

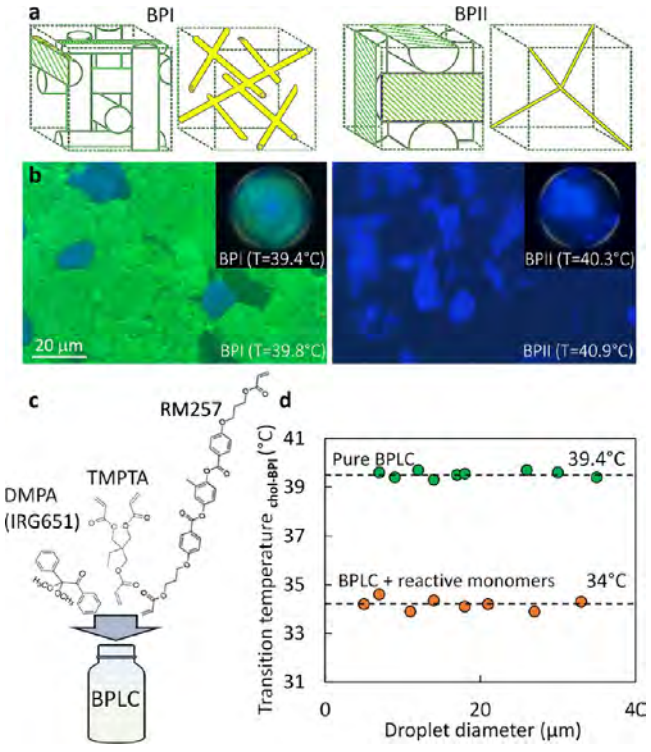

Figure 1. Transition temperatures of blue phases in the pure systems (in film and in droplet) and in the presence of reactive mesogens. (a) Schematic presentation of cubic unit cells and disclination lines in BPI and BPII. (b) Cross-polarized micrographs of BPI and BPII in a 12 μm thick film and a 20 μm droplet. (c) Reactive mixture components. (d) Chol-BPI transition temperature as a function of droplets size (μm) for the pure BPLC sample and reactive mixture.

Experimentally, BPs are generated by mixing a nematic liquid crystal (LC) with a chiral dopant. At room temperature, the resulting mixtures exhibit a chiral nematic phase, which is also known as the cholesteric phase (Chol), whose local director rotates along its perpendicular axis leading to a helical twisting structure. The cholesteric phase can be described by the pitch, p, which corresponds to the distance required for the director to complete a full 2π rotation.[10] At high levels of chirality, $p \lesssim 500$ nm, BPs appear in a narrow temperature range between the cholesteric and the isotropic phases (0.5–1.0 K). They typically form polycrystalline specimens, hindering their potential usefulness for applications. In order to widen the temperature range where BPs can form, past efforts have sought to incorporate additional components, namely polymers or nanoparticles, into the LC material.[9,12−22] These guest components tend to accumulate in the disclination lines of the host LC phase. This process lowers the free energy costs associated with the defects, thereby stabilizing the BP structure.[9,22] Polymer stabilization in bulk LCs has emerged as an effective means of expanding the stability range of chiral structures and BPs.[9,12,13,17,19,20] The polymer network acts as a template for the BPs with the director field fixed at the LC–polymer interface due to surface effects. The thermal stability of the templated BPs depends on numerous parameters, including polymer chain solubility, stiffness, composition, and cross-link density.[12,13,15,16,23] While several studies have examined polymerization of low chiral liquid crystals within microscale droplets, very little is known about BP stabilization in curved geometries.[15,24−28] Confining pure BPs in micrometer-sized droplets has recently been shown to slightly increase their stability temperature range.[29−32] Additional theoretical reports indicate that severe confinement in different geometries leads to the emergence of rich and complex BP-like configurations, including an array of line disclinations of double-helix shape, two orthogonal sets of parallel winding disclinations, and a regular array of ring defect.[33−36]

A key motivation behind this work has been to create a system in which we can generate crystal–crystal transformations in a material whose liquid-like nature makes it extremely responsive to physical and chemical stimuli. To do so, we combine the effect that confinement and polymerization have on the structure and stability of BPs. The rationale is that confinement in droplets, on the one hand, facilitates the formation of large BP monodomains.[30] On the other hand, polymerization significantly enhances thermal stability. By combining these two effects, we can produce BP droplets that exhibit a wide range of thermal stability and whose behavior can be controlled by manipulating the size.

Furthermore, since the BPs are polymerized, their optical response can be further controlled by strain. Importantly, the polymerization of the disclination lines does not produce a stiff polymer template, thereby allowing for reversible BP crystal–crystal transformations. We anticipate that the proposed system will find applications in photonics and metamaterials design.

RESULTS AND DISCUSSION

Polydisperse high chirality liquid crystal droplets, ranging from 5 to 60 μm, were prepared by vortex mixing followed by sonication. The phase transitions of the BPs were first examined for the pure LC sample (without containing reactive mesogens) using a polarized optical microscope in the reflection mode. Our results show that confining the BPs in spherical droplets can lower the BP transition temperatures (cholesteric-BPI, BPI-BPII, BPII-isotropic) relative to the same material in a 12 μm thick film (Figures 1b and S1). The phase transition temperatures of a 12 μm thick film were measured to be 39.8 and 40.9 °C for BPI and BPII, respectively (Figure 1b). The BPI and BPII phase transition temperatures in droplets were observed to be 39.4 and 40.3 °C, respectively (Figure 1b (inset)). Although the transition temperatures were slightly shifted, the BPs stability range remained unaffected (Figure S1). This slight reduction in the transition temperatures of BP microdroplets has been previously observed by Bukusoglu and co-workers and was attributed to the hydrolysis of the components.[32]

In the absence of UV light irradiation, we subsequently measured the phase-transition temperatures of droplets containing reactive mesogens. Incorporating the UV-reactive mesogens led to marked thermodynamic differences, including

https://doi.org/10.1021/acsnano.1c04231
ACS Nano 2021, 15, 15972−15981

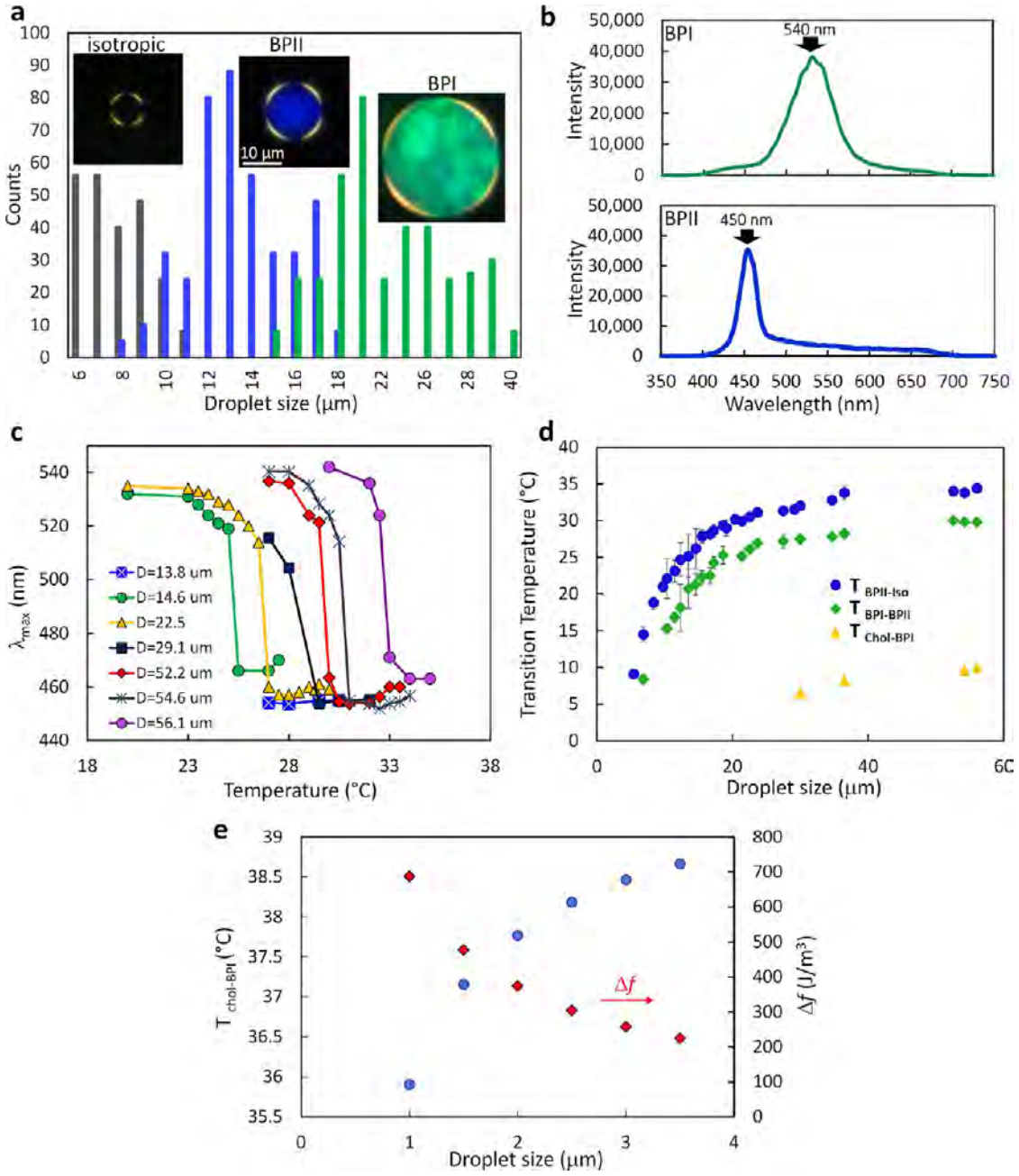

Figure 2. Droplet size effect on the phase transition of polymer-stabilized BP droplets. (a) Emerging stabilized mesophases as a function of droplet diameters. (b) Reflectance peaks of the droplets with BPI and BPII structures. (c) Evolution of the reflectance spectra as a function of temperature. (d) Transition temperatures and thermal stability region of the stabilized blue phases as a function of droplet size. (e) Theoretical prediction for nonpolymerized case. Chol-BPI transition temperature (left axis) and density of free energy difference (right axis) as a function of droplet diameter. The transition temperature increases asymptotically with the droplet size, converging to its value in bulk (~40 °C).

a drop of the cholesteric-BPI transition temperature of the mixture (Figure 1d). Moreover, the reactive liquid crystal mixture did not show the BPI-BPII phase transition during heating or cooling processes. To stabilize the structure of BPI in droplets, the reactive high chirality liquid crystal mixture was irradiated with UV light (wavelength of 365 nm and intensity of 33 mW/cm^2) for 45 min at a temperature where BPI is observed (Figure S2).

Surprisingly, polymerizing the reactive high chirality LC under spherical confinement resulted in optical features and phase behaviors that were size-correlated; *e.g.*, different BP structures were observed in droplets having different diameters (Figure 2). This intriguing feature should be contrasted with reports on polymerized BPs in films.[9,11,13,19] In our own experiments, for example, over the course of photopolymerization of BPI in a 12 μm thick sample cell, the BPI structure with multidomain texture was stabilized for a temperature range of 25−50 °C, which was confirmed by polarized optical microscopy in the reflection mode (Figure S3). Upon additional temperature increase, BPII was not observed, and the sample instead transitioned into the isotropic phase. This

https://doi.org/10.1021/acsnano.1c04231
ACS Nano 2021, 15, 15972−15981

behavior is consistent with literature results on polymer templating.[11,12]

To validate our observations and identify the lattice structure of the stabilized BPs in individual droplets, we used polarized optical microscopy combined with microspectroscopy. The reflection spectra of the stabilized mesophases were measured at room temperature (Figure 2b). After photopolymerization, the majority of the droplets having a diameter below 10 μm were found to be in the isotropic phase and did not exhibit any optical reflection. Droplets with diameters between 11 and 16 μm showed a distinct reflectance peak at approximately 450 nm, corresponding to the reflected color observed in the polarized image, which can be attributed to the Bragg diffraction from the [100] plane in BPII. Droplets larger than 17 μm in diameter, on the other hand, showed a strong reflectance peak of around 540 nm, which is consistent with the reflection spectra of the [110] plane in BPI. The broader reflectance peak in BPI can be attributed to the polycrystalline nature and nonuniform orientation of lattice planes in the droplets (Figure 2b). The size-dependent behavior, however, was altered by changing the polymerization time. With longer UV exposures, the centers of the droplet-size distributions in the isotropic, BPII, and BPI phases at room temperature were slightly shifted to larger diameters (Figure S4).

We further investigated the stabilized structures in the BP droplets. The changes with the temperature of the reflectance spectra of the stabilized BP droplets reveal that the polymerized scaffold is flexible and can undergo significant transformations. Specifically, we find that the polymerized BP structures can undergo a reversible transformation from BPI to BPII and *vice versa*. According to our spectroscopy measurements, larger droplets with the stabilized BPI structure exhibit reflectance peaks in the range of 520−540 nm. As the temperature is raised close to the BPI-BPII transition, the peak drops to the range of 480−510 nm. After the transition, there is a steep drop in the reflectance to about 430−450 nm (Figure 2c). The sharp drop in the reflectance results is indicative of a phase transition. This intriguing dynamic feature of the polymer-stabilized BPI droplets should be contrasted with the frozen polymer-templated behavior that occurs in bulk. In films or bulk, BPs grow into a polycrystalline sample, and the subsequent polymerization takes place in a variety of small and randomly oriented grains (Figure S3). Moreover, polymerized line defects in polycrystalline samples stabilize a given BP and hinder subsequent lattice transformations into another BP symmetry. In contrast, confinement into droplets facilitates uniform BP monodomain formation, and flexible polymerized networks are produced by the process proposed here. The transformation between polymer-stabilized BPs is then possible under spherical confinement. In this context, it is of interest to refer to the work of Li and Jin *et al.*, who identified the martensitic nature of the lattice transformation between BPs.[4,6] Using simulations, they could visualize how the disclination lines change from one BP symmetry into the other. The results presented here show that such a transformation is also possible when having the flexible and uniform networks provided by the polymerized disclination lines.

For the range of droplet diameters considered here, the transition temperatures of the BPs in both the pure and the reactive mixture are size-independent. The transition temperatures of the stabilized droplets are, however, strongly size-dependent; the larger the size of the droplets, the higher the transition temperature. The transition temperature increases asymptotically with the droplet size and levels off for large droplets (Figure 2d). It has been recently found that confining pure BPs in droplets can result in deformation of the cubic BP lattices, which can lead to a size-dependent phase behavior in LCs.[7,30,32] Note that while previous reports found the effect of droplet size on phase behavior for pure BPs to be small, past observations also suggest that a substantial temperature drop may take place as the droplet size decreases below 1 μm. Overall, a comparison of the confinement effects on the transition temperature of the stabilized BPs (Figure 2d) with that reported for the pure sample (Figure 1c in ref 32), indicates that incorporating the polymerizing substance into the disclination regions and stabilizing the BPs can shift the size dependency of the phase behavior to larger droplets and lower temperatures. In addition, comparing the transition temperatures of the BPs before (Figures 1b and S1) and after polymerization (Figure 2d), one can conclude that by stabilizing BPs within a spherical geometry, the stability window of BPI and BPII enhances to approximately 20 and 5 °C, respectively. While the transition temperatures of the stabilized droplets show a strong size-dependency, their stability range is independent of the droplet size (Figure 2d).

The effect of confinement and droplets size have also been reported for low chirality liquid crystals. Krakhalev *et al.* have shown the formation of double-helix structures with linear defects in a low chirality liquid crystal microdroplets with homeotropic surface anchoring, where decreasing the droplet size aligns the bipolar axis at a smaller angle to the aspect direction.[37] Using free energy minimization and topological theory, Sec *et al.* have demonstrated the formation of knotted and linked disclination loops in chiral liquid crystal droplets with homeotropic surface anchoring in which the variation in the pitch to the confinement ratio alters defects from knotted structures to a chiral state.[38] By confining chiral liquid crystals in shells with homeotropic anchoring, Tran *et al.* have shown the emergence of stripes engulfing perpendicular substripes and a focal conic domain (FCD). They have shown that while thin shells favor the bent structure, chiral structures in thick shells adopt a focal conic domain state.[39] Recently, Durey *et al.* have reported the formation of topological skyrmions and cholesteric fingers in Janus chiral liquid crystal shells. Upon reducing the shell thickness, they have observed transition from cholesteric fingers to skyrmion structures.[40]

To explain the effect of confinement on the formation of the BPs, we turn to a Landau de Gennes (LdG) theory for the director. We have recently shown that geometrical confinement increases the BP free energy and triggers a phase transition.[30] Under confinement, the transition temperatures of a BP droplet ($T_{iso} \rightarrow T_{BPII} \rightarrow T_{BPI} \rightarrow T_{chol}$) are different from those of the bulk. Considering that the equilibrium nematic order parameter S depends on T, and taking into account the strain induced by the confinement, if we take the unconfined (bulk) system as a reference, the temperature shift can be estimated from

$$\Delta T \approx \frac{4}{3a(S_D^2 - S_B^2)}\left(\Delta f - \frac{1}{4}B(S_D^3 - S_B^3) - \frac{9}{16}C(S_D^4 - S_B^4)\right) \quad (1)$$

where Δf is the LdG free energy density difference and S_B and S_D are the equilibrium nematic order parameters in the bulk and droplet, respectively. The material parameters are $a = 4 \times$

https://doi.org/10.1021/acsnano.1c04231
ACS Nano 2021, 15, 15972−15981

10^5 J m^{-3} K^{-1}, $B = -4 \times 10^6$ J m^{-3}K^{-1}, and $C = 4.26 \times 10^6$ J m^{-3} K^{-1}; for BPI, we take $S_B = 0.616$, and S_D changes slightly as a function of the droplet's diameter. The temperature shift for different droplet sizes is estimated using Δf and S_D obtained from simulations ($S_D \sim 0.635$). Our results clearly show that confinement reduces the bulk transition temperature (see Figure 2e). Our calculations are in agreement with previous reports, where a temperature shift of ∼2°C was observed for pure, 2 μm diameter BP droplets.[32] Moreover, it should be noted that our theoretical results predict a significant temperature shift for diameters $\lesssim 2$ μm, so the possibility of observing BPI or even BPII at room temperature for small enough drops cannot be ruled out.

Adding monomer increases the range of stability of the BPs, which can significantly lower the transition temperature and produce a similar but more notorious phenomenon than the one shown in Figure 2e; this is confirmed by the experimental data (Figure 2d). To explain this finding, we rely on Fukuda's work.[36] When a volume fraction, ϕ, of monomers agglomerate at the disclination lines of a BPI, they form cylindrical regions of volume Ω_M (Figure S5). Their resulting free energy is given by

$$F_{BPI}^{mono} = \int_{\Omega_{tot}-\Omega_M} d\boldsymbol{r} f(\boldsymbol{r}) + \Omega_{tot}(\phi f_M + \sigma s) \tag{2}$$

where $f(\boldsymbol{r})$ is the profile of the free energy density of the BPI, Ω_{Tot} is the total volume, and f_M is the free energy density contribution of the monomer, which is assumed to be position independent. The last term of eq 2 accounts for the effect of the interfacial energy that depends on the anchoring energy, σ, and the area per unit volume, s, of the cylindrical regions formed by the monomer aggregation at the disclination lines (Figure S5). In turn, the free energy of the cholesteric phase with monomers is given by

$$F_{Chol}^{mono} = \Omega_{Tot}[(1-f)f_{Chol} + \phi f_M] \tag{3}$$

where f_{Chol} is the density free energy of the pure cholesteric phase. From eqs 2 and 3, we have

$$F_{BPI}^{mono} - F_{Chol}^{mono} = \int_{\Omega Tot-\Omega M} d\boldsymbol{r} f(\boldsymbol{r}) + \Omega_{Tot} [-(1-\phi)f_{Chol} + \sigma s] \tag{4}$$

which shows that the stability of the BPI increases with monomer concentration. For chiral droplets, we have the combined effect of confinement and polymerization on the stability of BPs. According to Fukuda, an ideal, undistorted BPI unit cell of lattice parameter a_{BPI} contains straight disclination lines that can be seen as four diagonals of length $\sqrt{3}\,a_{BPI}$. Therefore, in each BP-unit cell, the monomer aggregation produces cylindrical regions of volume $4\sqrt{3}\,a_{BPI}\pi r^2$ which also corresponds to ϕa_{BPI}^3, whereby the area of the interface per unit volume can be given as

$$s = \frac{8\sqrt{3}\,a_{BPI}\pi r}{a_{BPI}^3} = \frac{4}{a_{BPI}}(\sqrt{3}\pi\phi)^{1/2} \tag{5}$$

The free energy gap between the monomer-laden BPI and cholesteric phase depends on the monomer volume fraction as (see Supporting Information)

$$F_{BPI}^{mono} - F_{Chol}^{mono} = F_{BPI} - F_{Chol} + \Omega_{Tot}\left[(f_{Chol} - f_{Iso})\phi + \frac{4\sigma}{a_{BPI}}(\sqrt{3}\pi\phi)^{1/2}\right] \tag{6}$$

with F_{BPI} and F_{Chol} representing the free energy of the pure BPI and the cholesteric phase. The integral in eq 4 is extended to the total volume by considering the monomer-rich disclination lines as locally isotropic regions. Since the isotropic phase has a larger free energy density than the cholesteric one, adding a monomer can stabilize BPI over the cholesteric phase. Confinement in droplets, on the other hand, distorts the BP unit cells. The disclination lines can bend close to the curved interface, expanding the BP unit cells.[7,30,32] Larger disclination lines per unit cell in curved confinement results in a larger interface area per unit volume $s^* \approx \frac{4}{a_{BPI}^*}(\sqrt{3}\pi\phi)^{1/2}$, with a_{BPI}^* being the average lattice parameter of the distorted BPI, which depends on the droplet size. Since $a_{BPI}^* > a_{BPI}$, a larger stability range is expected to be achieved for BPI under confinement (eq 6). For 1.5 μm diameter droplets, a lattice expansion of ∼6% has been reported, which reduces with increasing droplet size.[30] Therefore, the Chol-BPI transition temperature in droplets appears to be size-dependent, which is in quantitative agreement with our experimental results.

We have discussed how monomer aggregation at the disclination lines changes the Chol-BPI transition temperature. But how can a polymerized network undergo a reversible change to a network with a different topology? To answer this question, we refer to the martensitic nature of the BP crystals transformation. In the course of the BPI-BPII transition, DTCs, the building units of the BP crystals, exhibit a diffusionless behavior. Our large-scale simulations have recently shown that the disclination lines of BPI can bend and connect at specific locations to create the characteristic defect network of BPII.[4] Such a process can also be considered for flexible polymerized disclination lines.

We used conoscopy and super-resolution confocal laser scanning microscopy (super-resolution CLSM) to further explore the structural details of the stabilized BP droplets (Figures 3 and 4). The conoscopy technique to determine the Kossel diagrams is widely used to unveil periodic lattice planes and differentiate between BPI and BPII structures.[8,41−44] This characterization method is based on the diffraction patterns, which form on the back focal plane of the objective from monochromatic incident light. We used monochromatic light with a wavelength of 405 nm and an objective lens with a high numerical aperture (50×, NA = 0.7) to ensure that the sample is illuminated with a highly convergent light beam. However, to employ this method, we were limited by the size of the droplets; only droplets larger than 50 μm in diameter were large enough to produce visible diffraction patterns in the Kossel diagrams. Therefore, we were only able to exploit this technique on the large droplets having a BPI structure (Figure 3b). In addition, the optical effects associated with the geometrical curvature of the spherical droplets hindered the formation of distinct diffraction patterns. Nevertheless, comparing the Kossel diagram patterns in the representative droplet with the reference table reported by Hauser *et al.*[45] confirms the formation of a BPI structure with a multidomain nature and raises the possibility of the existence of planes with orientations of [110], [111], [211], and [200] (Figure 3b).

https://doi.org/10.1021/acsnano.1c04231
ACS Nano 2021, 15, 15972−15981

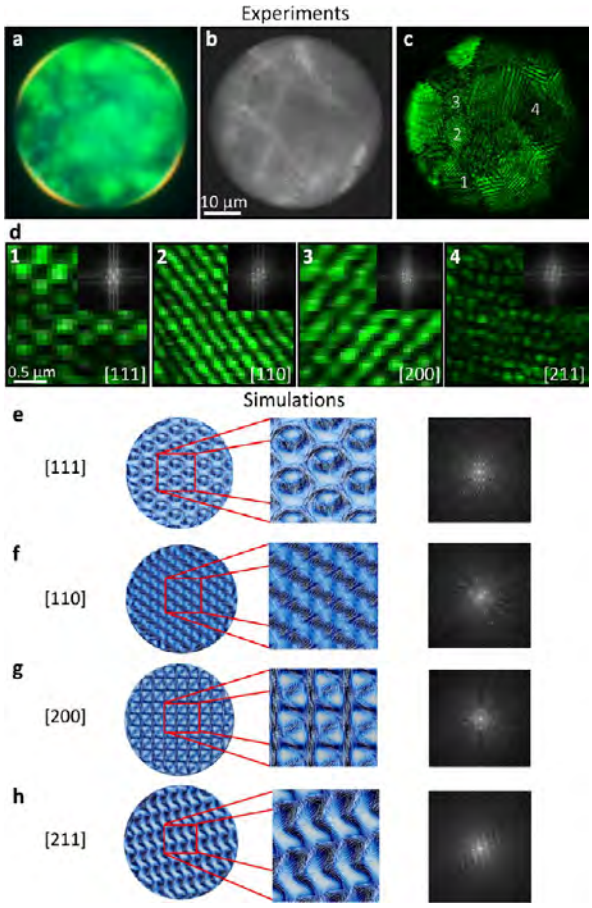

Figure 3. Lattice planes and periodic structure in a polymer-stabilized BPI droplet. (a) Polarized optical microscopy of the stabilized BPI in the reflection mode taken at room temperature. (b) Kossel diagram patterns of 52 μm BPI droplet. (c) Confocal laser scanning microscopy of a representative stabilized BPI droplet (the CLSM images correspond to a different droplet from the one shown in Figure 3a. (d) Magnified images of the four selected platelets in Figure 3c and the corresponding FFT images. (e−h) Simulation of the DTC arrangement of a BPI droplet; each row corresponds to the [*hkl*] lattice orientation indicated at the left, followed by a zoom-in of the director field and the FFT image of the corresponding BPI symmetry.

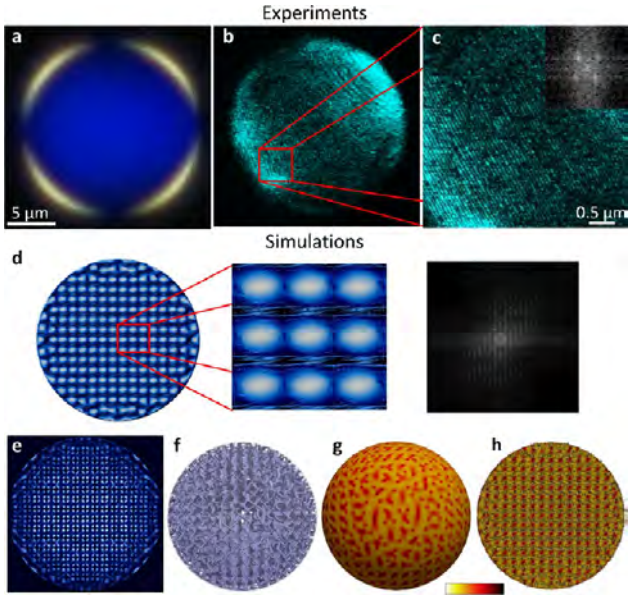

Figure 4. Lattice plane and periodic structure within a polymer-stabilized BPII droplet. (a) Polarized optical microscopy of the stabilized BPII in the reflection mode. (b) Confocal laser scanning microscopy of a stabilized BPII droplet. (c) Magnified image of the selected region in (b) and the corresponding FFT image. (d) Simulation of the DTC arrangement of a BPII droplet with a [100]-lattice orientation, followed by a zoom-in of the director field and the FFT-image of the BPII (100) symmetry. (e−h) Simulation results of a BPII droplet showing the [100]-lattice orientation: (e) micrograph, (f) disclination lines, (g) surface $\lambda^{-1/2}$ point defects, and (h), director field and defects of a slice at the droplet's equator.

Since the reflection behavior of all droplets follows the same patterns but at different temperatures, we can reliably expect the same to be true for the Kossel diagrams. These results were further confirmed by super-resolution CLSM and our computational simulation analysis.

Super-resolution CLSM allowed us to visualize the arrangement and periodic lattice structure of the double-twisted cylinders in the polymer-stabilized BP droplets in 3D real space. Although the periodic nature of the BP structures has been demonstrated before,[5,46] only a limited number of studies have succeeded in revealing the BP lattice structures in real space utilizing transmission electron microscopy (TEM)[47−49] and atomic force microscopy (AFM).[50] Such results, however, have been limited to the in-plane characterization and have been influenced by the fracture-induced topography modulation. Super-resolution CLSM, on the other hand, is an advanced and noninvasive technique to achieve three-dimensional structural images of the DTCs of the BPs in the original state and without undergoing any destructive processes. To the best of our knowledge, only one study has employed CLSM to observe BP structures in a polymerized liquid crystal film, and that report focused solely on a structural analysis of a stabilized BPI.[51]

To observe the periodic lattice structures, the CLSM was operated in the reflection mode with a narrow pinhole. In fact, the periodic lattice structure of BPs, which matches the wavelength of the Bragg diffractions, leads to a strong reflection pattern, which was detected by a photomultiplier tube. For stabilized BP droplets, imaging was conducted at room temperature, and for pure BP droplets, the samples were heated to the BPI and BPII phase transition temperatures. The strongest reflection pattern of the internal structures was achieved at the wavelengths of 543 nm (He−Ne laser) and 458 (Argon laser) for BPI and BPII droplets, respectively, which agrees with the spectroscopy measurements. The CLSM image at the equator of a stabilized BPI droplet exhibits a platelet texture with clear periodic patterns of DTCs that span several hundred nanometers (Figure 3c). Each platelet contains a uniform periodic pattern of DTCs separated from the neighboring domains by distinct grain boundaries. The arrangement of the DTCs in platelets reflects the cubic lattice symmetry of the BPI phase, and their orientation is associated with the bcc lattice planes and the polycrystalline structure of BPI. The lattice plane orientations were analyzed within several platelets. Four selected domains in Figure 3c are magnified in Figure 3d for better visualization. From the CLSM images, a lattice constant of $a = 260 \pm 7$ nm was measured for the bcc structure of BPI, and from the Fast Fourier Transform (FFT) analysis the lattice planes [111], [110], [200], and [211] were

https://doi.org/10.1021/acsnano.1c04231
ACS Nano 2021, 15, 15972−15981

proposed to describe the periodic arrangement of DTCs in domains 1, 2, 3, and 4, respectively. The presence of these lattice directions was qualitatively confirmed with the Kossel diagram patterns (Figure 3b). We also performed detailed computational studies on the arrangement of DTCs in BPs with different in-plane lattice orientations over an interface with planar anchoring. In agreement with Higashiguchi *et al.*,[51] our simulations indicate that CLSM images show the BP bulk structure, and the observed symmetries depend on the in-focus depth; they are not mirror reflections at the interface. Figures 3e–h show the simulation results, where each row is associated with a specific lattice orientation and is composed by a top view of the DTCs arrangement followed by a zoom-in of the director field of a bulk slice and the corresponding FFT image of the DTCs. We can observe from Figure 3d and e–h the correspondence between the CLSM images and the director field in the bulk of the droplet for each of the obtained BPI lattice orientations. From simulations, we can also extract a perspective about how the director field and the disclination lines behave in the proximity of a planar interface (Figure S6). Our simulations indicate that the [111] and [211] lattice orientations are accompanied by more distortions of the disclination lines, which is expected since, thermodynamically, $BPI_{(110)}$ and $BPI_{(200)}$ are more favored to form at planar interfaces.[32,52]

The super-resolution CLSM image for a single slice of a polymer stabilized BPII droplet displays a uniform periodic simple cubic arrangement of DTCs (Figure 4b). According to the FFT analysis, the periodic structure is aligned along the [100] plane and spans over the entire area (Figure 4c). For this arrangement, a lattice constant of $a = 150 \pm 9$ nm was measured from the CLSM images. The direction of the lattice plane can also be determined from the measured lattice constant and the selective reflection of the BPII droplet at a wavelength of 450 nm using $\lambda = \frac{2na}{\sqrt{h^2 + k^2 + l^2}}$, where n is the refractive index, a is the lattice unit cell constant, and h, k, l are Miller indices.

The small size of the droplets in the stabilized BPII prevented Kossel diagram measurements. Simulation results of a $BPII_{(100)}$ in the proximity of a planar interface, where the director field exhibits a simple cubic array of double-twisted cylinders, are in quantitative agreement with the experimental observations (Figure 4d). While the disclination lines (and consequently the BPII cells) deform at the interface, the internal structure remains unchanged (Figure 4f).

Comparing CLSM images of the stabilized BPI and BPII droplets (Figure 3c and Figure 4b) reveals distinct differences in the formation of perfectly aligned and monodomain BP structures. While stabilized BPI droplets exhibit a multidomain texture with distinct grain boundaries, the BPII droplet adopts a perfect, single-crystal internal structure. Imaging the stabilized BPII droplets in the axial direction confirms that the uniform alignment and single-crystalline structure are preserved throughout the volume and extend throughout the entire droplet. Movies of the internal structure of the droplets can be found in the Supporting Information (Supplementary Movies S1 and S2, z-stacks, step size = 80 nm). We have explained in previous work that for BPs in contact with degenerate planar anchoring surfaces, there is a favorable out-of-plane lattice orientation.[8,52] Thus, starting from the isotropic phase, when lowering the temperature the BPII nucleates and grows with the [111]-plane parallel to the substrate. In contrast, the BPI follows the [110] lattice orientation—the [200] is the second favorable lattice orientation. Confinement in droplets having planar anchoring conditions assists the uniform nucleation and growth of BPII, which in addition to the simple cubic symmetry of this phase, favors the formation of a single-crystalline structure (see Figure 4a,b). Interestingly, the BPII droplet has a macroscopic single crystal inside, with no evidence of lattice distortions in the droplet's bulk (Figure 4b). Our simulations give us additional insights into what is happening in this case. Parts e–h of Figure 4 show the simulation micrographs and the characteristic disclination lines of a BPII droplet viewed from the [100] lattice orientation. The disclination lines deform in the vicinity of the droplet interface, which results in a noncrystalline array of topological defects at the surface of the droplet (Figure 4g). Inside the droplet, however, a well-ordered BPII structure forms, which is confirmed by our experiments (Figure 4h, Figure 4b and Supplementary Movie S2).

For BPI, the droplet interface theoretically favors the $BPI_{(110)}$. However, given the BPI lattice symmetry, there are different possibilities for the in-plane lattice orientation;[6] in the absence of precisely patterned substrates, there is no control over the nucleation and growth, and therefore, other grains with different out-plane lattice orientations appear. As we have mentioned before, the BPII-BPI crystal transformation has been proven to be martensitic in nature; since the polymerized disclination lines are not stiff, this lattice transformation in the stabilized droplets is plausible.[4,6] Our experimental results confirm the reversibility and dynamic feature of the stabilized BPs confined in the spherical droplets when the temperature varies from the BPII to the BPI regime and vice versa.

CONCLUSION

We have studied the structure and phase behavior of polymer-stabilized BPs confined into spherical droplets. We have shown that photopolymerizing a mixture of reactive mesogens and a high chirality LC within droplets at a temperature at which BPI is observed stabilizes different BP structures. At room temperature, large droplets contain stabilized-BPI, while small droplets favor BPII and isotropic phases. The polymerized scaffold in the confined BPs can undergo reversible transformations, with BP structures that transition from the simple cubic symmetry in BPII to the body-centered cubic symmetry in BPI and vice versa as temperature varies. There is no precedent in the literature for the reversible dynamic in stabilized BPs observed here under spherical confinement. Our observations are in contrast to the "frozen-in" polymer-templated behavior that has been reported for the bulk. We have also found a pronounced size-dependence of the transition temperature in the stabilized BP droplets, which we have explained by relying on a Landau de Gennes description of the free energy of the system. The stability range of stabilized BPs is increased considerably by polymerization, but the range itself is independent of size. We achieve ranges of approximately 20 and 5 °C for BPI and BPII, respectively. Importantly, we have found that the stabilized BPII droplets adopt a perfect, single-crystal internal structure. In contrast, the stabilized BPI droplets exhibit a polydomain texture with distinct grain boundaries. Taken together, the results presented in this work serve to demonstrate that polymer stabilization of BP structures in droplets offers a promising platform for creation of single-crystal blue phases that can be rearranged reversibly and that are stable over a wide range of

https://doi.org/10.1021/acsnano.1c04231
ACS Nano 2021, 15, 15972–15981

temperatures, thereby offering opportunities for applications in optical technologies.

METHODS

Experiments. For this study, the nematic liquid crystal MLC 2142 and chiral dopant (4-(1-methylheptyloxycarbonyl)phenyl-4-hexyloxybenzoate (S-811)) were purchased from EMD Performance Materials Corp. To achieve a chiral liquid crystal capable of forming BPs (Figure 1a,b), the nematic liquid crystal (MLC 2142) was mixed with 35 wt % of the chiral dopant (S-811) using toluene as a solvent. Toluene was then evaporated from the mixture using a rotary evaporator. The UV reactive precursor was composed of 5.17 wt % trimethylol propane triacrylate (TMPTA, Aldrich), 7.49 wt % 4-(3-Acryloyloxypropyloxy)benzoesure 2-methyl-1,4-phenylester (RM257), 0.75 wt % DMPA (IRG65, Aldrich) as a photoinitiator, and 86.59 wt % of the high chirality liquid crystal (Figure 1c). In the absence of UV light irradiation, the mixture was heated beyond isotropic temperature for 1 h and stored overnight at room temperature to ensure complete dissolution and homogeneity of the components.

Droplets were formed by dispersing 10 μL of reactive BP mixture in 500 μL mQ-water. Poly(vinyl alcohol) (PVA, average molecular weight, M_w = 35−50k, 87−89% hydrolyzed) was then added to the mixture to stabilize the droplets in the aqueous solution and to induce planar surface anchoring. The droplet size of the LC emulsion ranged from 5 to 60 μm. The emulsion was dispersed in a circular well made out of polydimethylsiloxane, PDMS, film with a thickness of 100 μm, which was plasma bonded on a glass slide (Figure S2). To photopolymerize, the reactive emulsion was exposed to UV light irradiation (365 nm) at 0.5 °C above the temperature at which the reactive high chirality liquid crystal in the droplets shows BPI optical appearance (34.5 °C) (Figure 1d). The temperature of the emulsion was controlled by a hot stage (Linkam T120) to maintain the emulsion in BPI during the photopolymerization.

Polarizing microscopy images were obtained using the Olympus BX51-P. Reflection spectra were acquired using the FLAME-S-VIS-NIR-ES spectrometer. Leica SP5 AOBS TCS tandem scanner spectral confocal microscopy (super-resolution confocal laser scanning microscopy (CLSM)) with 100× oil objective lens was used to image the periodic structure of the BPs confined in the spherical droplets. For imaging, the label-free polymer-stabilized BP droplets were dispersed in 3% PVA aqueous solution. We added 1 wt % Borax to the aqueous solution to cross-link the PVA and prevent movement of the polymerized droplets during the confocal imaging process. The sample cell was covered with a cover glass (no. 1) and illuminated with He−Ne laser at the wavelengths of 543 and 633 nm as well as an argon laser at the wavelengths of 458, 488, and 514 nm. To observe the periodic lattice structures, the CLSM was operated in the reflection mode with a narrow pinhole. When the periodic lattice structure of BPs matches the wavelength of the laser beams, it leads to a strong Bragg reflection pattern, which was detected by a photomultiplier tube.

Continuum Simulations. A Landau−de Gennes mean-field theoretical approach was successfully used to model confined LCs. Under this framework, the free energy, F, of the system is a function of the symmetric and traceless tensor, $\mathbf{Q}$. For uniaxial systems, $Q_{ij} = S(n_i n_j - 1/3\ \delta_{ij})$, where S is the scalar order parameter and n_i are the components of the local director vector (i, j = 1,2,3). $F(\mathbf{Q})$ accounts for short-range contributions (f_{LdG}), long-range elastic contributions (f_E), and surface contributions (f_S). The free energy can be written as

$$F(\mathbf{Q}) = \int d^3x[f_{LdG}(\mathbf{Q}) + f_E(\mathbf{Q})] + \int d^2x f_S(\mathbf{Q}) \quad (7)$$

Stable and metastable configurations were obtained by minimization of the free energy functional according to the Ginzburg−Landau method as explained in the Supporting Information.

ASSOCIATED CONTENT

Supporting Information

The Supporting Information is available free of charge at https://pubs.acs.org/doi/10.1021/acsnano.1c04231.

Continuum simulations details, photopolymerization setup, phase-transition temperatures diagram of BPs measured in 20 mm films and droplets, stabilized mesophases size dependency for droplets polymerized upon 90 min of UV light irradiation, optical microscopy of stabilized BPI film, sketch of a polymerized disclination line of a BPI cell, simulation micrographs, director field and disclination lines for top and lateral views of different BPI lattice orientations (PDF)

z-stack scanning of periodic structure of DTCs in a polymer-stabilized BPI droplet using super-resolution CLSM (AVI)

z-stack scanning of periodic structure of DTCs in a polymer-stabilized BPII droplet using super-resolution CLSM (AVI)

AUTHOR INFORMATION

Corresponding Author

Juan J. de Pablo − *Pritzker School of Molecular Engineering, University of Chicago, Chicago, Illinois 60637, United States; Argonne National Laboratory, Lemont, Illinois 60439, United States;* orcid.org/0000-0002-3526-516X; Email: depablo@uchicago.edu

Authors

Monirosadat Sadati − *Pritzker School of Molecular Engineering, University of Chicago, Chicago, Illinois 60637, United States; Department of Chemical Engineering, Swearingen Engineering Center, University of South Carolina, Columbia, South Carolina 29208, United States;* orcid.org/0000-0001-9701-9637

Jose A. Martinez-Gonzalez − *Facultad de Ciencias, Universidad Autónoma de San Luis Potosí, San Luis Potosí 78295 SLP, Mexico;* orcid.org/0000-0001-7257-8889

Alexander Cohen − *Pritzker School of Molecular Engineering, University of Chicago, Chicago, Illinois 60637, United States*

Sepideh Norouzi − *Department of Chemical Engineering, Swearingen Engineering Center, University of South Carolina, Columbia, South Carolina 29208, United States*

Orlando Guzmán − *Departamento de Física, Universidad Autonóma Metropolitana, Ciudad de México 09340, Mexico*

Complete contact information is available at: https://pubs.acs.org/10.1021/acsnano.1c04231

Author Contributions

#M.S. and J.A.M.-G. contributed equally to this work. M.S. and J.J.d.P. conceived, and M.S. performed experiments. J.A.M.-G., O.G and J.J.d.P. conceived and performed numerical simulations and theoretical calculations. M.S., J.A.M.-G. and J.J.d.P. wrote the manuscript. J.J.d.P. guided the work. A. Cohen and S. Norouzi contributed to performing the experiments and writing the manuscript. All authors have given approval to the final version of the manuscript.

Notes

The authors declare no competing financial interest.

https://doi.org/10.1021/acsnano.1c04231
ACS Nano 2021, 15, 15972−15981

ACKNOWLEDGMENTS

The authors acknowledge the support given by the Department of Energy, Office of Basic Energy Sciences, Division of Materials Science and Engineering, under grant DE-SC0019762. The calculations presented in this work were carried out on the GPU cluster at the University of Chicago, supported by the National Science Foundation under MRI Grant No. 1828629. M.S. acknowledges the support from SC EPSCoR under Grant No. 21-GE03. JAM-G additional computer resources as well as technical advice and support were provided by the Laboratorio Nacional de Supercómputo del Sureste de México (LNS), a member of the CONACYT national laboratories, under Project No. 201901023N.

REFERENCES

(1) Randle, V. Grain Boundary Engineering: An Overview after 25 Years. *Mater. Sci. Technol.* **2010**, *26* (3), 253−261.
(2) Palumbo, G.; Lehockey, E. M.; Lin, P. Applications for Grain Boundary Engineered Materials. *JOM* **1998**, *50*, 40−43.
(3) Gao, Y.; Zhang, Y.; Beeler, B. W.; Wang, Y. Self-Organized Multigrain Patterning with Special Grain Boundaries Produced by Phase Transformation Cycling. *Phys. Rev. Mater.* **2018**, *2*, 073402.
(4) Li, X.; Martínez-González, J. A.; Hernández-Ortiz, J. P.; Ramírez-Hernández, A.; Zhou, Y.; Sadati, M.; Zhang, R.; Nealey, P. F.; De Pablo, J. J. Mesoscale Martensitic Transformation in Single Crystals of Topological Defects. *Proc. Natl. Acad. Sci. U. S. A.* **2017**, *114* (38), 10011−10016.
(5) Li, X.; Martínez-González, J. A.; Guzmán, O.; Ma, X.; Park, K.; Zhou, C.; Kambe, Y.; Jin, H. M.; Dolan, J. A.; Nealey, P. F.; De Pablo, J. J. Sculpted Grain Boundaries in Soft Crystals. *Sci. Adv.* **2019**, *5* (11), eaax9112.
(6) Jin, H. M.; Li, X.; Dolan, J. A.; Joseph Kline, R.; Martínez-González, J. A.; Ren, J.; Zhou, C.; de Pablo, J. J.; Nealey, P. F. Soft Crystal Martensites: An *in Situ* Resonant Soft X-Ray Scattering Study of a Liquid Crystal Martensitic Transformation. *Sci. Adv.* **2020**, *6* (13), eaay5986.
(7) Sadati, M.; Martinez-Gonzalez, J. A.; Zhou, Y.; Qazvini, N. T.; Kurtenbach, K.; Li, X.; Bukusoglu, E.; Zhang, R.; Abbott, N. L.; Hernandez-Ortiz, J. P.; DePablo, J. J. Prolate and Oblate Chiral Liquid Crystal Spheroids. *Sci. Adv.* **2020**, *6* (28), eaba6728.
(8) Martínez-González, J. A.; Li, X.; Sadati, M.; Zhou, Y.; Zhang, R.; Nealey, P. F.; De Pablo, J. J. Directed Self-Assembly of Liquid Crystalline Blue Phases into Ideal Single-Crystals. *Nat. Commun.* **2017**, *8*, 15854.
(9) Kikuchi, H.; Yokota, M.; Hisakado, Y.; Yang, H.; Kajiyama, T. Polymer-Stabilized Liquid Crystal Blue Phases. *Nat. Mater.* **2002**, *1* (1), 64−68.
(10) Kitzerow, H.-S.; Bahr, C. *Chirality in Liquid Crystals*; Springer Springer-Verlag: New York, 2001; pp 186−218.
(11) Coles, H. J.; Pivnenko, M. N. Liquid Crystal Blue Phases with a Wide Temperature Range. *Nature* **2005**, *436* (7053), 997−1000.
(12) Castles, F.; Day, F. V.; Morris, S. M.; Ko, D. H.; Gardiner, D. J.; Qasim, M. M.; Nosheen, S.; Hands, P. J. W.; Choi, S. S.; Friend, R. H.; Coles, H. J. Blue-Phase Templated Fabrication of Three-Dimensional Nanostructures for Photonic Applications. *Nat. Mater.* **2012**, *11* (7), 599−603.
(13) Castles, F.; Morris, S. M.; Hung, J. M. C.; Qasim, M. M.; Wright, A. D.; Nosheen, S.; Choi, S. S.; Outram, B. I.; Elston, S. J.; Burgess, C.; Hill, L.; Wilkinson, T. D.; Coles, H. J. Stretchable Liquid-Crystal Blue Phase Gels. *Nat. Mater.* **2014**, *13* (8), 817−821.
(14) Gharbi, M. A.; Manet, S.; Lhermitte, J.; Brown, S.; Milette, J.; Toader, V.; Sutton, M.; Reven, L. Reversible Nanoparticle Cubic Lattices in Blue Phase Liquid Crystals. *ACS Nano* **2016**, *10* (3), 3410−3415.
(15) Yan, Q.; Wei, Z.; Lin, P.; Cheng, Z.; Pu, M.; Huang, Z.; Lin, W. Polymer Stabilized Cholesteric Liquid Crystal Particles with High Thermal Stability. *Opt. Mater. Express* **2018**, *8* (6), 1536.
(16) Fan, C. Y.; Jau, H. C.; Lin, T. H.; Yu, F. C.; Huang, T. H.; Liu, C.; Sugiura, N. Influence of Polymerization Temperature on Hysteresis and Residual Birefringence of Polymer Stabilized Blue Phase LCs. *J. Disp. Technol.* **2011**, *7* (11), 615−618.
(17) Rahman, M. A.; Said, S. M.; Balamurugan, S. Blue Phase Liquid Crystal: Strategies for Phase Stabilization and Device Development. *Sci. Technol. Adv. Mater.* **2015**, *16* (3), 033501.
(18) Wang, L.; He, W.; Xiao, X.; Meng, F.; Zhang, Y.; Yang, P.; Wang, L.; Xiao, J.; Yang, H.; Lu, Y. Hysteresis-Free Blue Phase Liquid Crystal Stabilized by ZnS Nanoparticles. *Small* **2012**, *8* (14), 2189−2193.
(19) Xiang, J.; Lavrentovich, O. D. Blue Phase Polymer-Templated Nematic with Sub-Millisecond Broad-Temperature Range Electro-Optic Switching. *Appl. Phys. Lett.* **2013**, *103* (5), 051112.
(20) Yan, J.; Wu, S.-T. Polymer-Stabilized Blue Phase Liquid Crystals: A Tutorial [Invited]. *Opt. Mater. Express* **2011**, *1* (8), 1527.
(21) Kizhakidathazhath, R.; Higuchi, H.; Okumura, Y.; Kikuchi, H. Effect of Polymer Backbone Flexibility on Blue Phase Liquid Crystal Stabilization. *J. Mol. Liq.* **2018**, *262*, 175−179.
(22) Yoshida, H.; Tanaka, Y.; Kawamoto, K.; Kubo, H.; Tsuda, T.; Fujii, A.; Kuwabata, S.; Kikuchi, H.; Ozaki, M. Nanoparticle-Stabilized Cholesteric Blue Phases. *Appl. Phys. Express* **2009**, *2* (12), 121501.
(23) Kizhakidathazhath, R.; Higuchi, H.; Okumura, Y.; Kikuchi, H. Effect of Polymer Backbone Flexibility on Blue Phase Liquid Crystal Stabilization. *J. Mol. Liq.* **2018**, *262*, 175−179.
(24) Shi, Y.; Zhu, T.; Zhang, T.; Mazzulla, A.; Tsai, D. P.; Ding, W.; Liu, A. Q.; Cipparrone, G.; Sáenz, J. J.; Qiu, C. W. Chirality-Assisted Lateral Momentum Transfer for Bidirectional Enantioselective Separation. *Light: Sci. Appl.* **2020**, *9* (1), 2047−7538.
(25) Hernández, R. J.; Provenzano, C.; Mazzulla, A.; Pagliusi, P.; Viola, M.; Cipparrone, G. Cholesteric Solid Spherical Microparticles: Chiral Optomechanics and Microphotonics. *Liq. Cryst. Rev.* **2016**, *4* (1), 59−79.
(26) Lee, S. S.; Kim, J. B.; Kim, Y. H.; Kim, S. H. Wavelength-Tunable and Shape-Reconfigurable Photonic Capsule Resonators Containing Cholesteric Liquid Crystals. *Sci. Adv.* **2018**, *4* (6), 8276−8298.
(27) Heo, I. S.; Park, S. Y. Smart Shell Membrane Prepared by Microfluidics with Reactive Nematic Liquid Crystal Mixture. *Sens. Actuators, B* **2017**, *251*, 658−666.
(28) Lee, H. G.; Munir, S.; Park, S. Y. Cholesteric Liquid Crystal Droplets for Biosensors. *ACS Appl. Mater. Interfaces* **2016**, *8* (39), 26407−26417.
(29) Lin, P.; Wei, Z.; Yan, Q.; Chen, Y.; Wu, M.; Xie, J.; Zeng, M.; Wang, W.; Xu, J.; Cheng, Z. Blue Phase Liquid Crystal Microcapsules: Confined 3D Structure Inducing Fascinating Properties. *J. Mater. Chem. C* **2019**, *7* (16), 4822−4827.
(30) Martínez-González, J. A.; Zhou, Y.; Rahimi, M.; Bukusoglu, E.; Abbott, N. L.; De Pablo, J. J. Blue Phase Liquid Crystal Droplets. *Proc. Natl. Acad. Sci. U. S. A.* **2015**, *112* (43), 13195−13200.
(31) Lin, J. De; Daniel Ho, Y. L.; Chen, L.; Lopez-Garcia, M.; Jiang, S. A.; Taverne, M. P. C.; Lee, C. R.; Rarity, J. G. Microstructure-Stabilized Blue Phase Liquid Crystals. *ACS Omega* **2018**, *3* (11), 15435−15441.
(32) Bukusoglu, E.; Wang, X.; Martinez-Gonzalez, J. A.; De Pablo, J. J.; Abbott, N. L. Stimuli-Responsive Cubosomes Formed from Blue Phase Liquid Crystals. *Adv. Mater.* **2015**, *27* (43), 6892−6898.
(33) Fukuda, J. I.; Žumer, S. Structural Forces in Liquid Crystalline Blue Phases. *Phys. Rev. E - Stat. Nonlinear, Soft Matter Phys.* **2011**, *84* (4), 040701.
(34) Fukuda, J. I.; Žumer, S. Quasi-Two-Dimensional Skyrmion Lattices in a Chiral Nematic Liquid Crystal. *Nat. Commun.* **2011**, *2* (1), 1−5.
(35) Fukuda, J. I.; Žumer, S. Novel Defect Structures in a Strongly Confined Liquid-Crystalline Blue Phase. *Phys. Rev. Lett.* **2010**, *104* (1), 017801.
(36) Fukuda, J. I. Stabilization of a Blue Phase by a Guest Component: An Approach Based on a Landau-de Gennes Theory. *Phys. Rev. E - Stat. Nonlinear, Soft Matter Phys.* **2010**, *82* (6), 061702.

https://doi.org/10.1021/acsnano.1c04231
ACS Nano 2021, 15, 15972−15981

(37) Krakhalev, M. N.; Gardymova, A. P.; Prishchepa, O. O.; Rudyak, V. Y.; Emelyanenko, A. V.; Liu, J. H.; Zyryanov, V. Y. Bipolar Configuration with Twisted Loop Defect in Chiral Nematic Droplets under Homeotropic Surface Anchoring. *Sci. Rep.* **2017**, *7* (1), 1−10.
(38) Seč, D.; Čopar, S.; Žumer, S. Topological Zoo of Free-Standing Knots in Confined Chiral Nematic Fluids. *Nat. Commun.* **2014**, *5* (1), 1−7.
(39) Tran, L.; Lavrentovich, M. O.; Durey, G.; Darmon, A.; Haase, M. F.; Li, N.; Lee, D.; Stebe, K. J.; Kamien, R. D.; Lopez-Leon, T. Change in Stripes for Cholesteric Shells *via* Anchoring in Moderation. *Phys. Rev. X* **2017**, *7* (4), 041029.
(40) Durey, G.; Sohn, H. R. O.; Ackerman, P. J.; Brasselet, E.; Smalyukh, I. I.; Lopez-Leon, T. Topological Solitons, Cholesteric Fingers and Singular Defect Lines in Janus Liquid Crystal Shells. *Soft Matter* **2020**, *16* (11), 2669−2682.
(41) Scharf, T. *Polarized Light in Liquid Crystals and Polymers*; John Wiley & Sons, Inc: Hoboken, NJ, 2006; pp 168−182. DOI: 10.1002/047007437x.
(42) Miller, R.; Gleeson, H. Cubic Liquid Crystal Blue Phases. *J. Phys. II* **1996**, *6* (6), 909−922.
(43) Chen, H. Y.; Hsieh, Y. C. Lattice Structure in Liquid-Crystal Blue Phase with Various Chiral Concentrations. *Liq. Cryst.* **2015**, *42* (10), 1472−1477.
(44) Fukuda, J.-I.; Nych, A.; Ognysta, U.; Žumer, S.; Muševič, I. Liquid-Crystalline Half-Skyrmion Lattice Spotted by Kossel Diagrams. *Sci. Rep.* **2018**, *8*, 17234.
(45) Hauser, A.; Thieme, M.; Saupe, A.; Heppke, G.; Krüerke, D. Surface-Imaging of Frozen Blue Phases in a Discotic Liquid Crystal with Atomic Force Microscopy. *J. Mater. Chem.* **1997**, *7* (11), 2223−2229.
(46) Kikuchi, H.; Izena, S.; Higuchi, H.; Okumura, Y.; Higashiguchi, K. A Giant Polymer Lattice in a Polymer-Stabilized Blue Phase Liquid Crystal. *Soft Matter* **2015**, *11* (23), 4572−4575.
(47) Tanaka, S.; Yoshida, H.; Kawata, Y.; Kuwahara, R.; Nishi, R.; Ozaki, M. Double-Twist Cylinders in Liquid Crystalline Cholesteric Blue Phases Observed by Transmission Electron Microscopy. *Sci. Rep.* **2015**, *5* (1), 16180.
(48) Zasadzinski, J. A. N.; Meiboom, S.; Sammon, M. J.; Berreman, D. W. Freeze-Fracture Electron-Microscope Observations of the Blue Phase III. *Phys. Rev. Lett.* **1986**, *57* (3), 364−367.
(49) Delacroix, H.; Gilli, J. M.; Erk, I.; Mariani, P. Structure Analysis of a Quenched Blue Phase I Using Electron Microscopy. *Phys. Rev. Lett.* **1992**, *69* (20), 2935−2938.
(50) Dumoulin, H.; Pieranski, P.; Delacroix, H.; Erk, I.; Gilli, J. M.; Lansac, Y. Compared Study of a Quenched Blue Phase by Direct Transmission Electron and Atomic Force Microscopy. *Mol. Cryst. Liq. Cryst. Sci. Technol., Sect. A* **1995**, *262* (1), 221−233.
(51) Higashiguchi, K.; Yasui, K.; Kikuchi, H. Direct Observation of Polymer-Stabilized Blue Phase I Structure with Confocal Laser Scanning Microscope. *J. Am. Chem. Soc.* **2008**, *130* (20), 6326−6327.
(52) Li, X.; Martínez-González, J. A.; Park, K.; Yu, C.; Zhou, Y.; De Pablo, J. J.; Nealey, P. F. Perfection in Nucleation and Growth of Blue-Phase Single Crystals: Small Free-Energy Required to Self-Assemble at Specific Lattice Orientation. *ACS Appl. Mater. Interfaces* **2019**, *11* (9), 9487−9495.

https://doi.org/10.1021/acsnano.1c04231
ACS Nano 2021, 15, 15972−15981